Science Advances
AAAS

Supplementary Materials for

Global concurrent climate extremes exacerbated by anthropogenic climate change

Sha Zhou *et al*.

Corresponding author: Sha Zhou, shazhou21@bnu.edu.cn

Sci. Adv. **9**, eabo1638 (2023)
DOI: 10.1126/sciadv.abo1638

This PDF file includes:

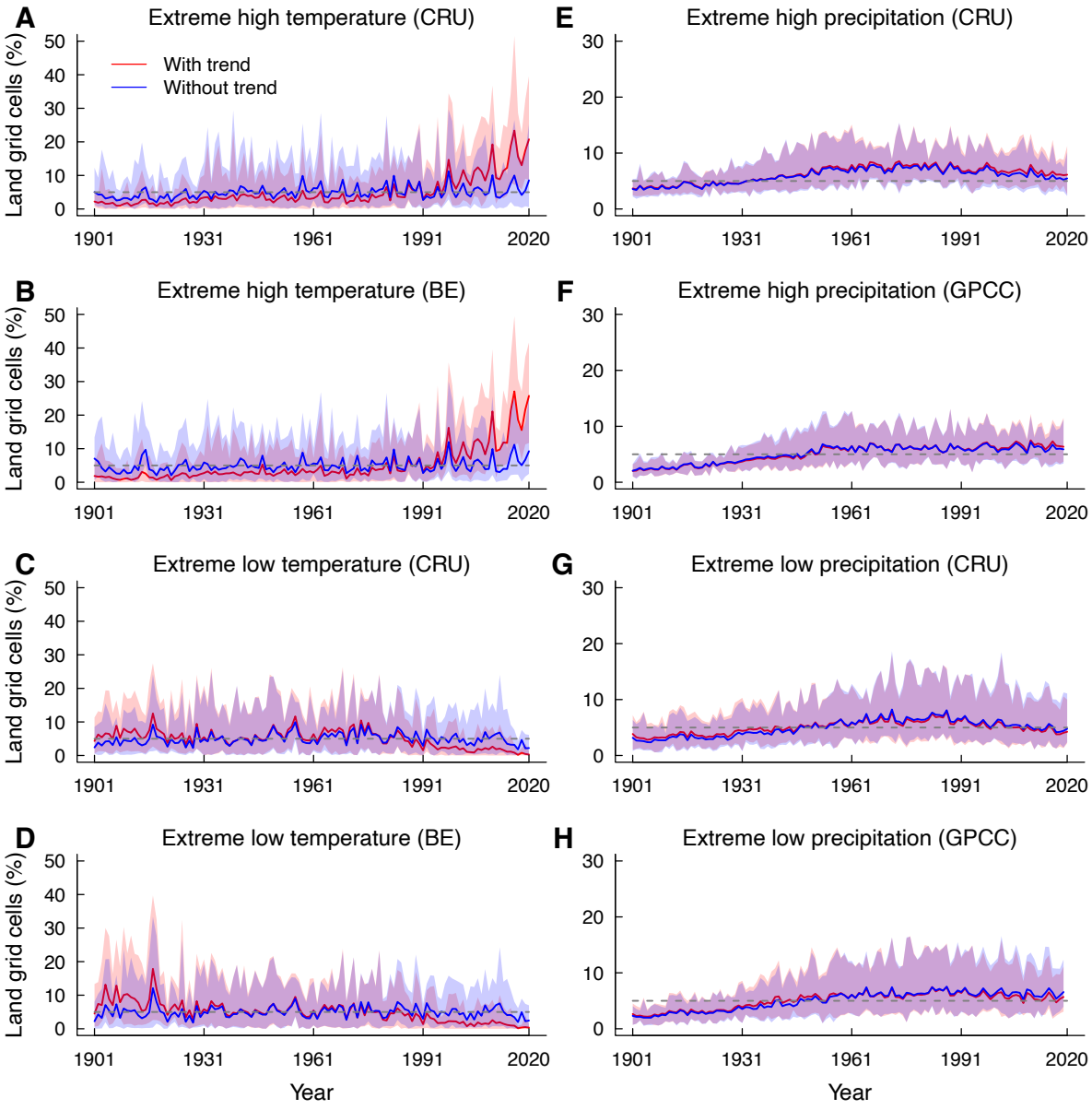

Fig. S1. Prevalence of concurrent climate extremes in observational datasets. (**A-D**) Proportion of land grid cells experiencing monthly extreme high (**A**,**B**) and extreme low (**C**,**D**) temperature during the period of 1901-2020 using CRU and Berkeley Earth (BE) temperature products. Climate extremes are identified using temperature (precipitation) data with and without long-term trends, which are defined as the mean temperature (precipitation) of a 20-year moving window. The solid lines show the mean monthly proportion, and the upper and lower bounds of the shading indicate the maximum and minimum monthly proportion for each year. The grey dashed lines show the expected proportion (5%) when occurrence of climate extremes is independent among different grid cells. (**E-H**) The same as (**A-D**), but for extreme high (**E**,**F**) and extreme low (**G**,**H**) precipitation using CRU and GPCC precipitation products.

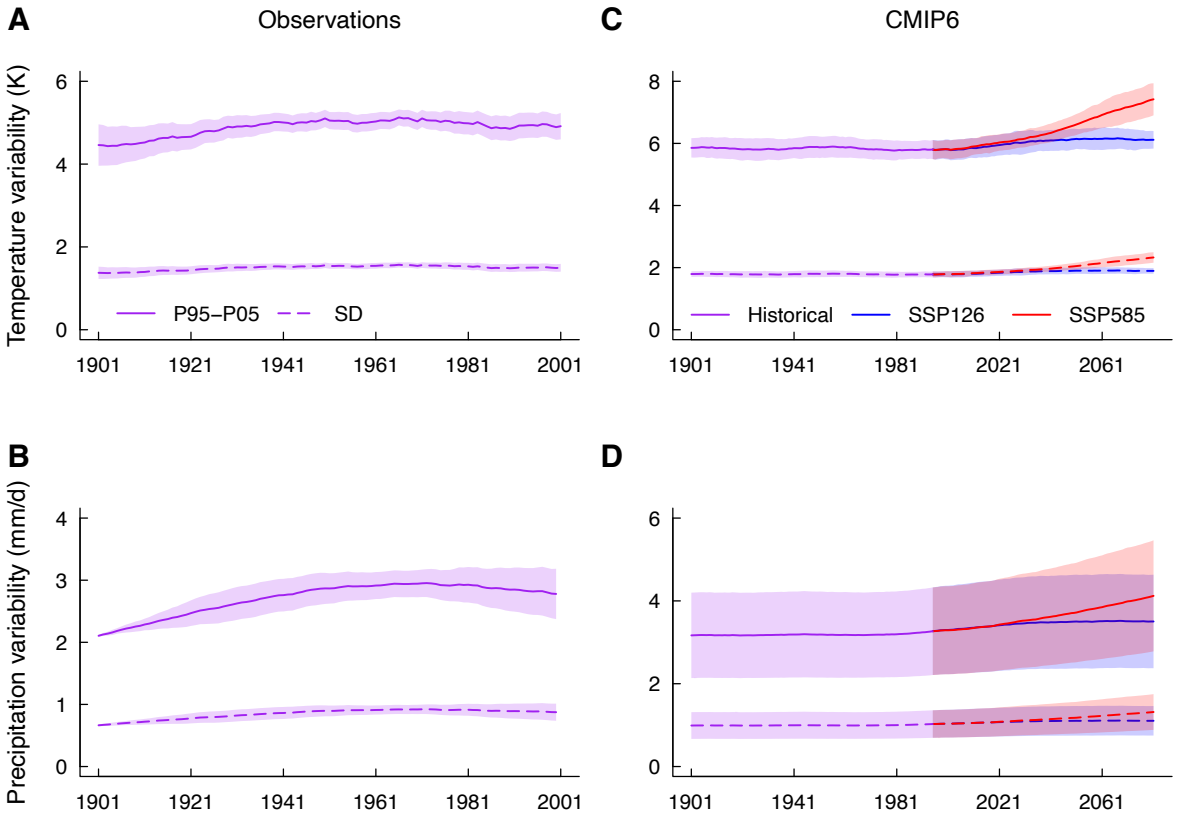

Fig. S2. Time-evolving global mean climate variability over land in observations and CMIP6 model simulations. (**A**,**B**) Global mean climate variability assessed by the difference between 95th percentile and 5th percentile (P95-P05, solid lines) and the standard deviation (SD, dashed lines) of deseasonalized and detrended climate variables from observational datasets. P95-P05 and SD are calculated for each land grid cell over a 20-year moving window (the first year is shown in the horizontal axes). (**C**,**D**) The same as (**A**,**B**), but from historical, SSP126, and SSP585 simulations of 11 GCMs in CMIP6. The shading shows the standard deviation of the results across observational datasets/models.

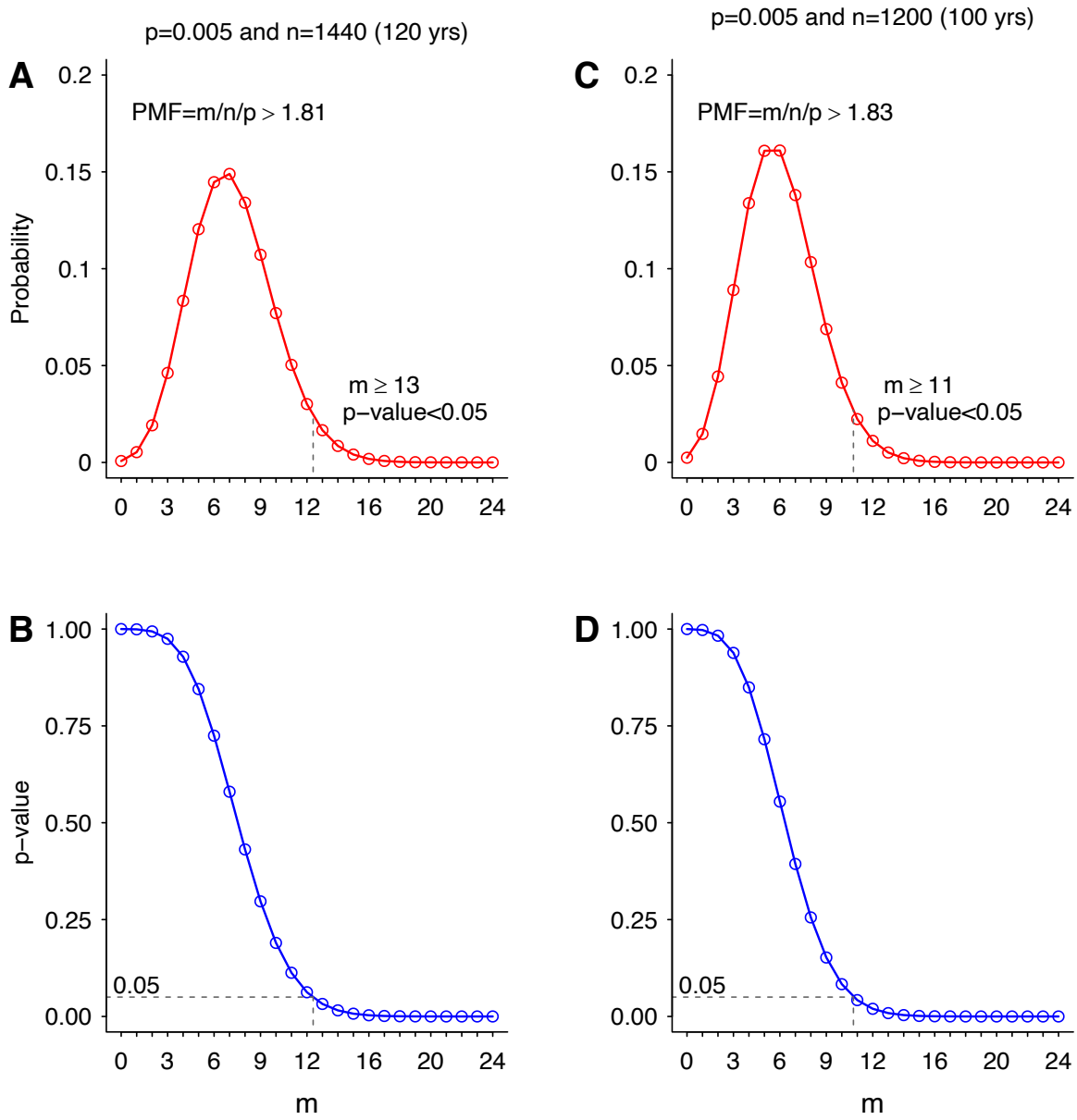

Fig. S3. Probability density function and the *p*-value of the binomial distribution with m as the number of occurrences. (**A**,**B**) 120 years (1440 months). (**C**,**D**) 100 years (1200 months).

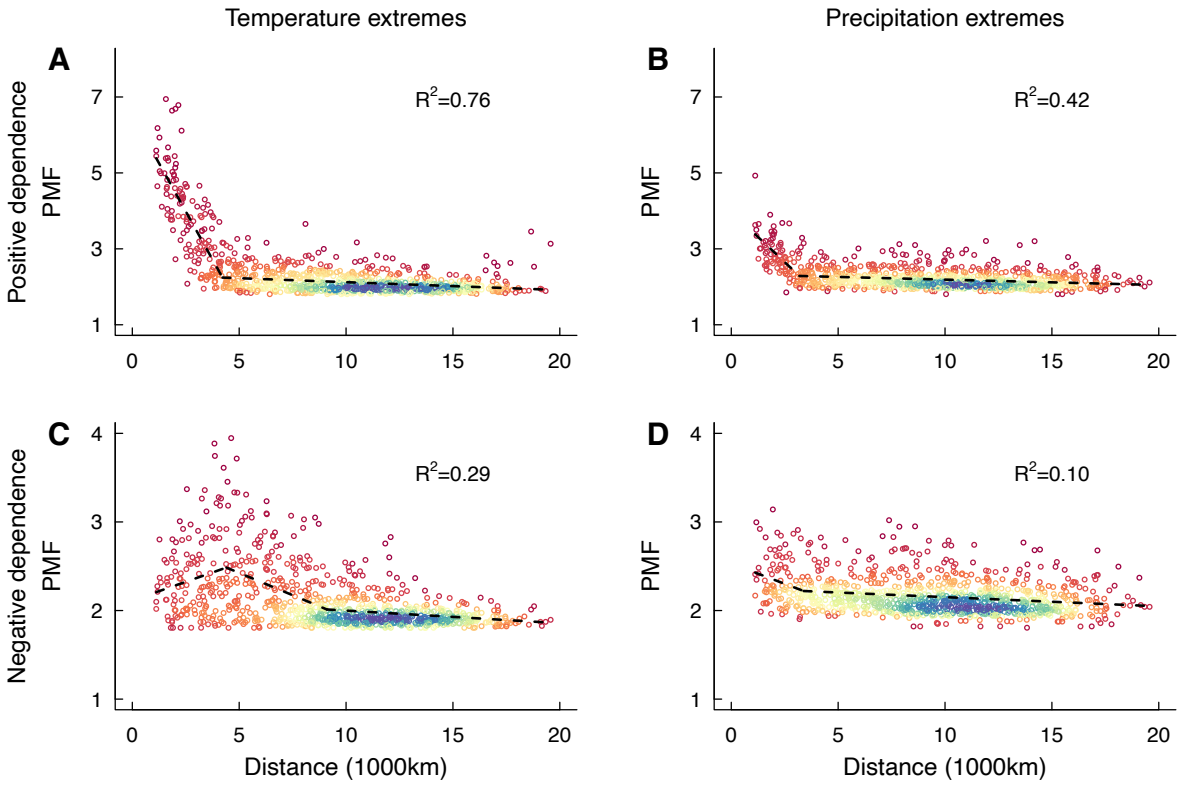

Fig. S4. Geographical distribution of spatially concurrent climate extremes. (A-D) The decrease in regional probability multiplication factor (PMF) of climate extremes with increase in the distance between the centers of each region pair based on observations without long-term trends during 1901-2020. Center location of these AR6 regions is listed in Table S2. The spectral color shows the density of points, with higher density in blue/purple and lower density in red. The coefficient of determination (R^2) for the segmented linear regression is shown for each panel.

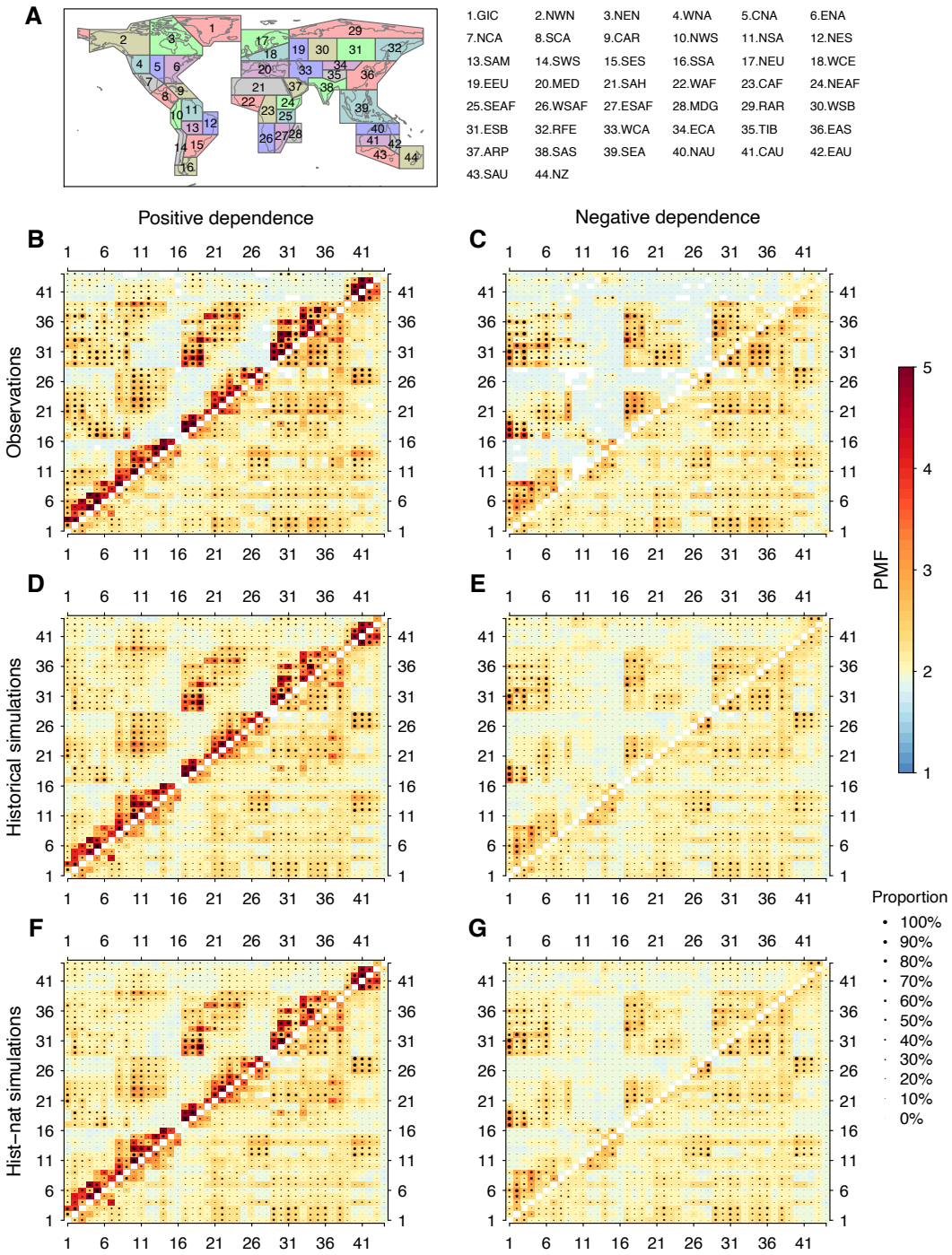

Fig. S5. Global pattern of spatially concurrent climate extremes in observational datasets and CMIP6 simulations. (**A**) IPCC AR6 climate reference land regions (excluding Antarctica). (**B**,**C**) The mean probability multiplication factor (PMF) for positively (**B**) and negatively (**C**) dependent climate extremes between pairs of 44 AR6 regions (top-left triangle: temperature extremes; bottom-right triangle: precipitation extremes) using observations without long-term trends during 1901-2020. Stippling denotes the proportion of grid cell pairs for which climate extremes are tested to be positively or negatively dependent in each AR6 region pair. (**D**-**G**) The same as (**B**,**C**), but for historical (**D**,**E**) and hist-nat (**F**,**G**) simulations of 11 GCMs in CMIP6.

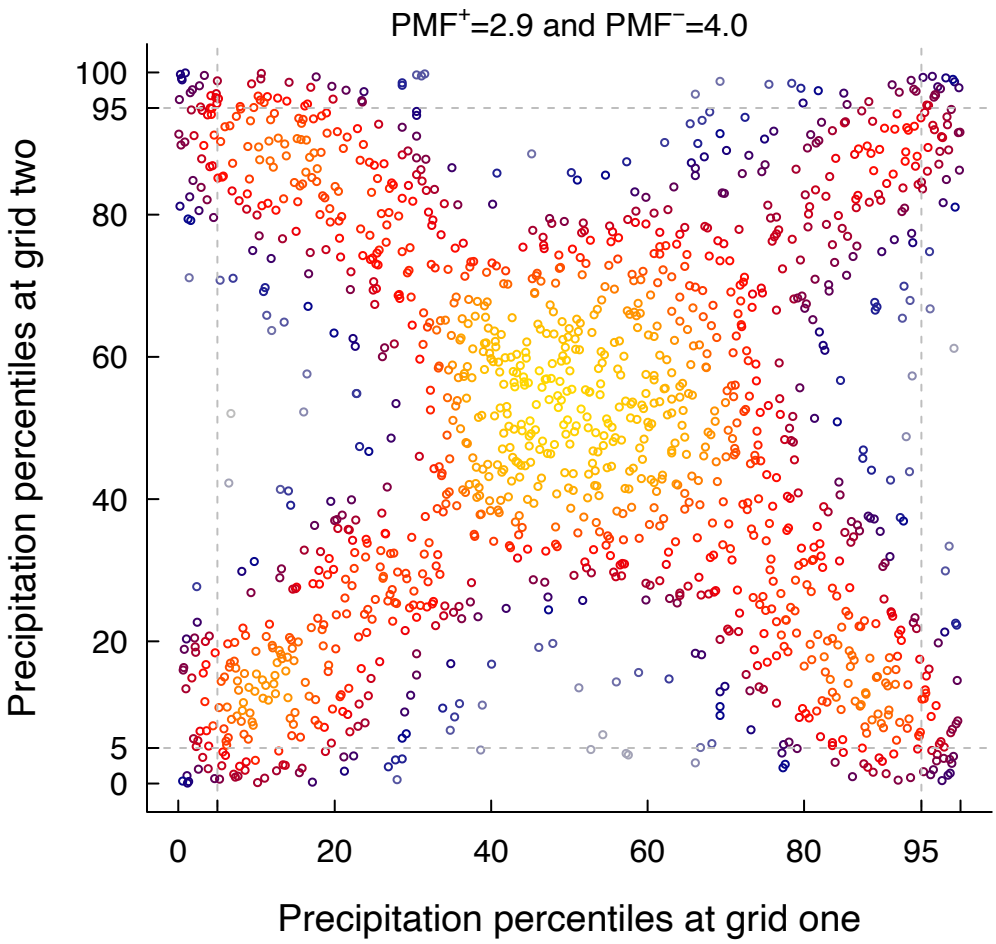

Fig. S6. An example of precipitation distribution for two grid cells. Precipitation extremes co-occur positively (PMF^{+}=2.9) and negatively (PMF^{-}=4.0) at these two grid cells.

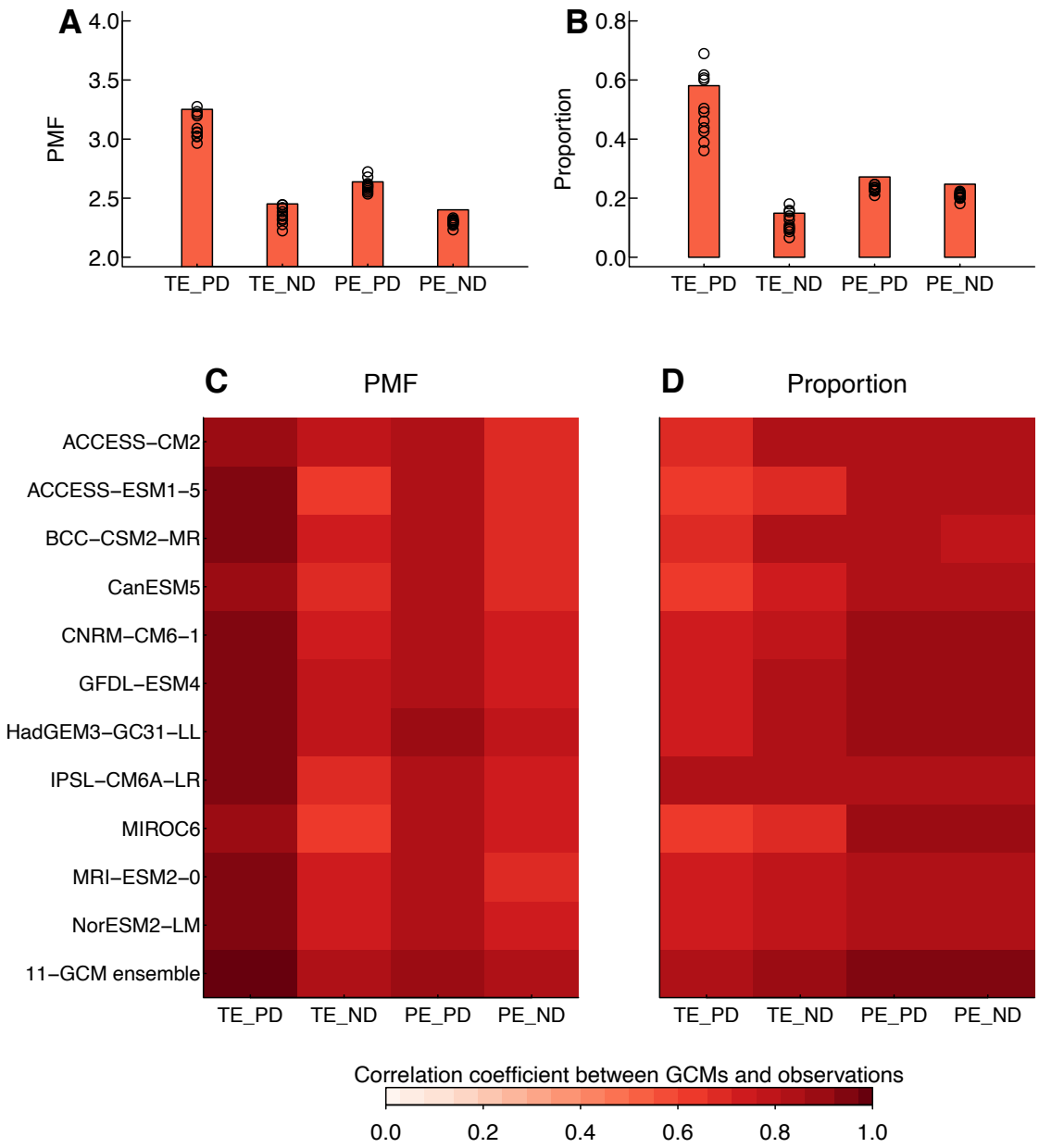

Fig. S7. Comparison of global concurrent climate extremes between CMIP6 models and the observations. (**A**) The global mean probability multiplication factor (PMF) for positively dependent temperature extremes (TE_PD), negatively dependent temperature extremes (TE_ND), positively dependent precipitation extremes (PE_PD), and negatively dependent precipitation extremes (PE_ND). The red bars show the mean results from the observations and the circles show results from the 11 GCMs in CMIP6. (**B**) The same as (**A**) but for the proportion of land grid cell pairs in which climate extremes are tested to be significantly dependent. (**C**) Correlation coefficient of PMF for the global pattern of concurrent climate extremes among all the pairs of 44 AR6 regions between CMIP6 models and the observations. (**D**) The same as (**C**) but for the correlation coefficient of the proportion grid cell pairs in which climate extremes are tested to be significantly dependent among the AR6 region pairs.

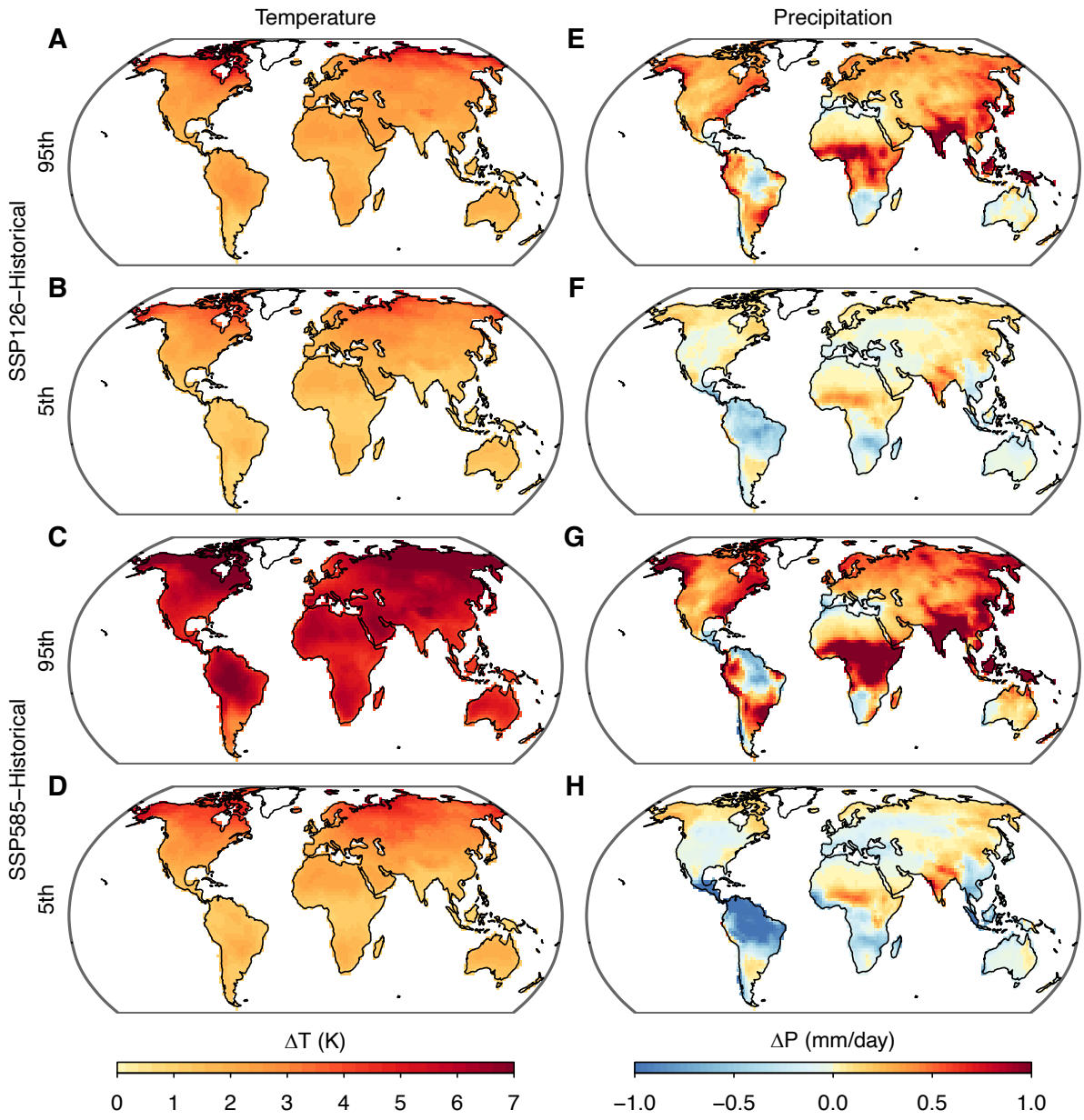

Fig. S8. Changes in the thresholds of climate extremes from historical (1901-2000) to future (2001-2100) periods. (**A**-**D**) Temperature thresholds. (**E**-**H**) Precipitation thresholds.

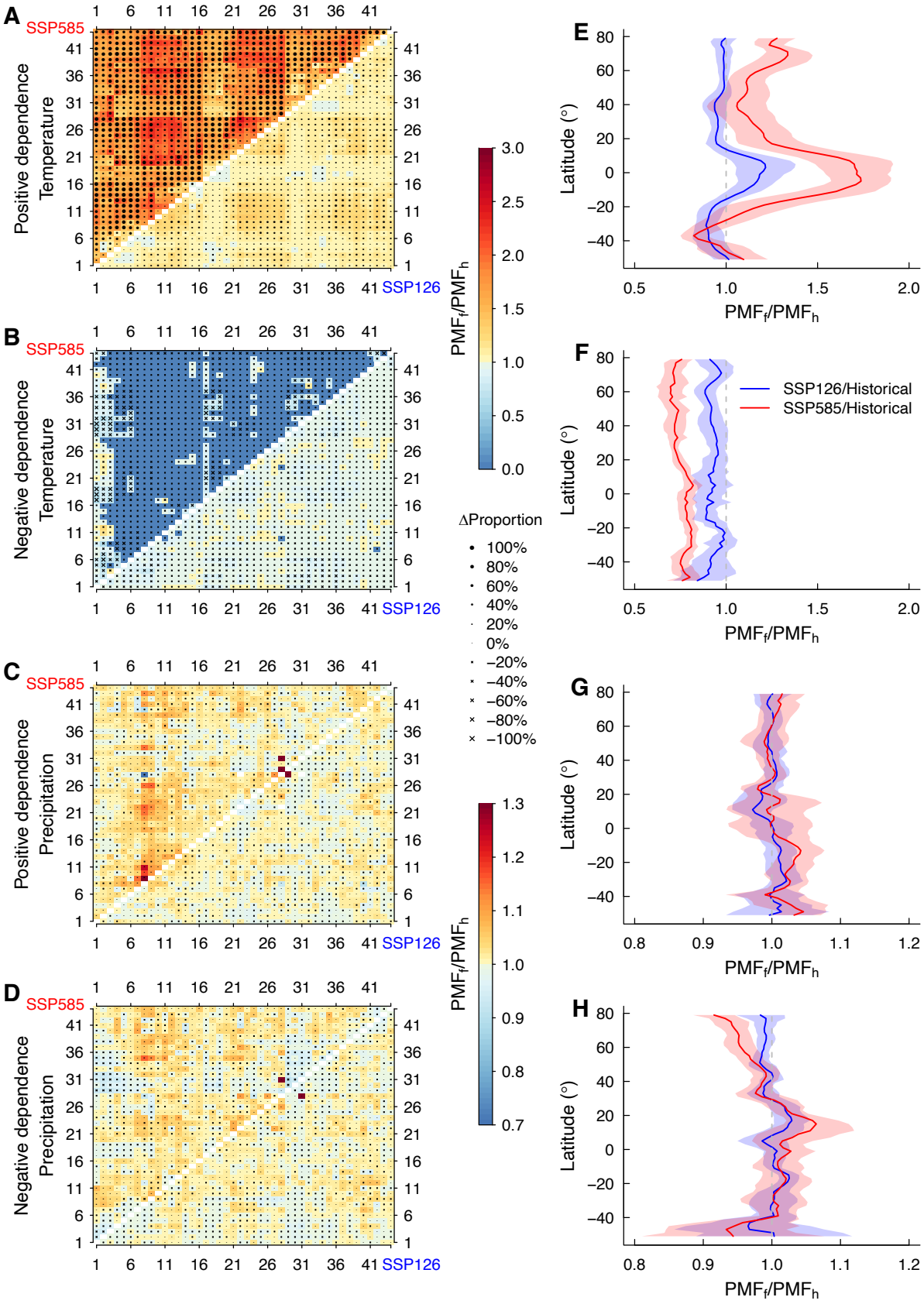
A
SSP585
SSP126
Positive dependence
Temperature
B
Negative dependence
Temperature
C
Positive dependence
Precipitation
D
Negative dependence
Precipitation
1 6 11 16 21 26 31 36 41
PMFf/PMFh
3.0
2.5
2.0
1.5
1.0
0.5
0.0
ΔProportion
100%
80%
60%
40%
20%
0%
−20%
−40%
−60%
−80%
−100%
1.3
1.2
1.1
1.0
0.9
0.8
0.7
E
F
G
H
Latitude (°)
80
60
40
20
0
−20
−40
0.5
1.0
1.5
2.0
0.8
0.9
1.0
1.1
1.2
PMFf/PMFh
SSP126/Historical
SSP585/Historical

Fig. S9. Projected increases in global concurrent climate extremes in CMIP6. (**A**-**D**) The ratio of regional probability multiplication factor in SSP126 and SSP585 (2001-2100, top-left triangle: SSP585; bottom-right triangle: SSP126) over historical (1901-2000) simulations (PMF_f/PMF_h). Climate extremes are identified according to individual thresholds for each of historical and future simulations. Stippling denotes changes in the proportion of grid cell pairs in which climate extremes are tested to be positively or negatively dependent in each AR6 region pair. (**E**-**H**) The latitudinal pattern of PMF_f/PMF_h between grid cell pairs within each 10° (5x2°) moving zonal band in SSP126 and SSP585 relative to historical simulations. The solid lines are multi-model mean of PMF_f/PMF_h and the shading shows the standard deviation of PMF_f/PMF_h across the 11 GCMs in CMIP6.

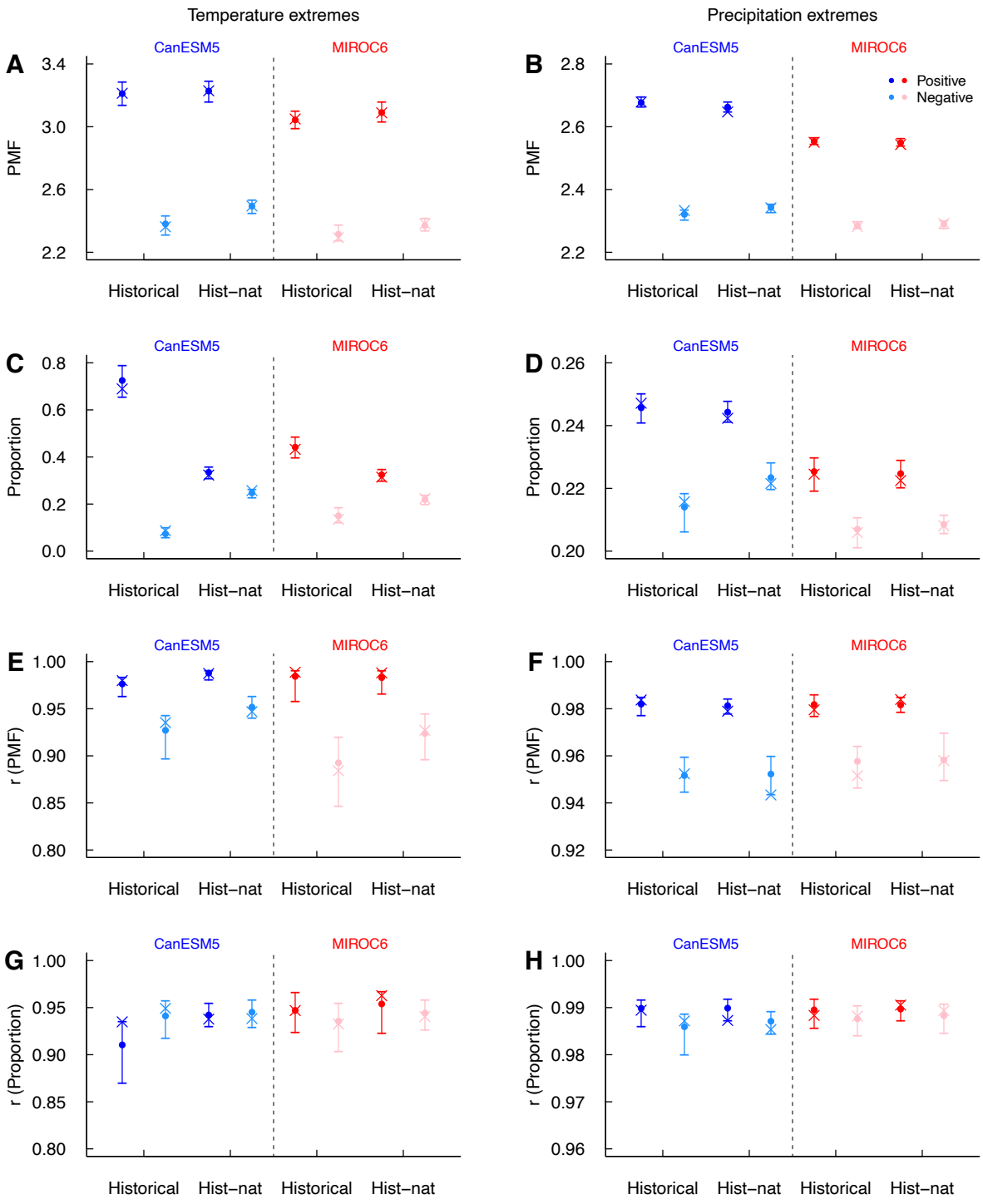

Fig. S10. Variations in global concurrent climate extremes among the 25 realizations of CanESM5 and the 50 realizations of MIROC6. (**A**,**B**) The global mean probability multiplication factor (PMF) for positively and negatively dependent climate extremes across all grid cells over land in historical and hist-nat simulations. (**C**,**D**) The same as (**A**,**B**), but for the proportion of land grid cell pairs with dependent climate extremes. (**E**,**F**) Correlation coefficient (r) between inter-region PMF (sample size: 946 pairs of regions) for each realization and the 946

averages using all realizations for both historical and hist-nat simulations. (**G**,**H**) The same as (**E**,**F**), but for the proportion of grid cell pairs with dependent climate extremes. In each panel, the multi-realization mean value (solid dot), the maximum and minimum values (short horizontal line), and the value for the first realization (r1i1p1f1, cross) are shown.

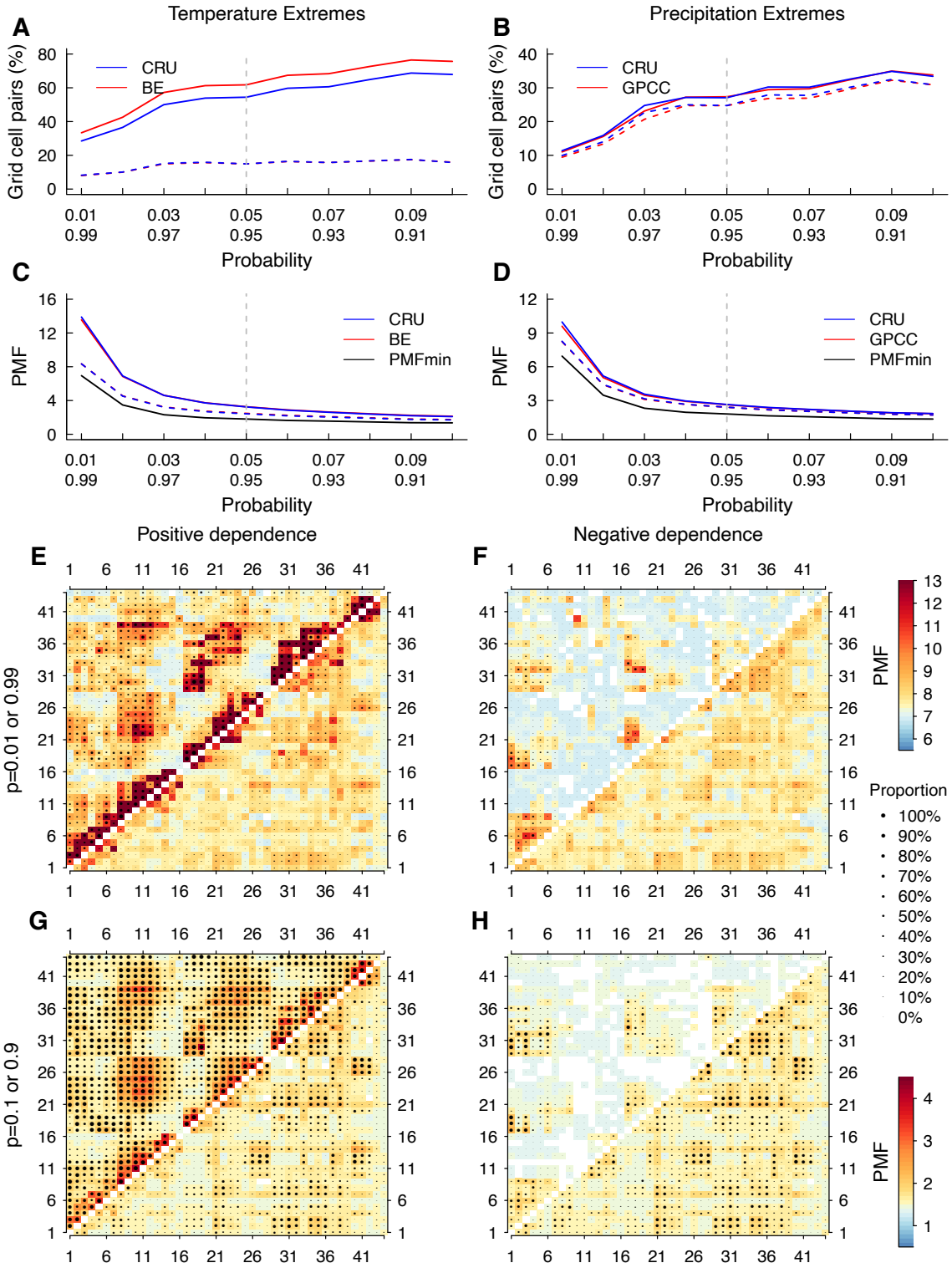

Fig. S11. Sensitivity of spatial dependence of climate extremes to the thresholds of climate extremes in observational products. (**A**,**B**) The proportion of land grid cell pairs in which climate extremes are tested to be positively (solid lines) and negatively (dashed lines) dependent when climate extremes are defined according to a series of probability thresholds from 0.9/0.1 to

0.99/0.01 using observations during 1901-2020. (**C**,**D**) The same as (**A**,**B**), but for the mean probability multiplication factor (PMF) for positively (solid lines) and negatively (dashed lines) dependent climate extremes. (**E**,**F**) The mean PMF for positively (**E**) and negatively (**F**) dependent climate extremes between AR6 regions (top-left triangle: temperature extremes; bottom-right triangle: precipitation extremes). Climate extremes are defined as months when climate anomalies are above their 99th percentiles or below their 1st percentiles. Label refers to AR6 regions from 1 to 44. Stippling denotes the proportion of grid cell pairs in which climate extremes are tested to be significantly dependent in each AR6 region pair. (**G**,**H**) The same as (**E**,**F**), but climate extremes are defined as months when climate anomalies are above their 90th percentiles or below their 10th percentiles.

Table S1. List of CMIP6 models used in this study.

Model	Ensemble	Institution
ACCESS-CM2	r1i1p1f1	Commonwealth Scientific and Industrial Research Organization (CSIRO) Australian Research Council Centre of Excellence for Climate System Science (ARCCSS)
ACCESS-ESM1-5	r1i1p1f1	Commonwealth Scientific and Industrial Research Organization (CSIRO)
BCC-CSM2-MR	r1i1p1f1	Beijing Climate Center (BCC)
CanESM5	r1i1p1f1	Canadian Center for Climate Modeling and Analysis (CCCma)
CNRM-CM6-1	r1i1p1f2	Centre National de Recherches Météorologiques (CNRM) Centre Européen de Recherche et Formation Avancée en Calcul Scientifique (CERFACS)
GFDL-ESM4	r1i1p1f1	NOAA Geophysical Fluid Dynamics Laboratory
HadGEM3-GC31-LL	r1i1p1f3	Met Office Hadley Centre (additional HadGEM2-ES realizations contributed by Instituto Nacional de Pesquisas Espaciais)
IPSL-CM6A-LR	r1i1p1f1	Institut Pierre Simon Laplace (IPSL)
MIROC6	r1i1p1f1	Japan Agency for Marine-Earth Science and Technology (JAMSTEC) Atmosphere and Ocean Research Institute (AORI) National Institute for Environmental Studies (NIES) RIKEN Center for Computational Science (R-CCS)
MRI-ESM2-0	r1i1p1f1	Meteorological Research Institute (MRI)
NorESM2-LM	r1i1p1f1	NorESM Climate modeling Consortium (NCC)

Table S2. List of the 44 land regions and the center location of these regions.

No.	Region Names		Latitude	Longitude
1	GIC	Greenland/Iceland	74.93°N	42.74°W
2	NWN	N.W.North-America	63.40°N	131.06°W
3	NEN	N.E.North-America	64.35°N	85.00°W
4	WNA	W.North-America	42.43°N	115.35°W
5	CNA	C.North-America	40.15°N	97.59°W
6	ENA	E.North-America	41.80°N	77.78°W
7	NCA	N.Central-America	27.32°N	106.16°W
8	SCA	S.Central-America	15.06°N	89.19°W
9	CAR	Caribbean	21.00°N	74.88°W
10	NWS	N.W.South-America	1.77°S	75.85°W
11	NSA	N.South-America	0.92°N	62.03°W
12	NES	N.E.South-America	10.10°S	43.48°W
13	SAM	South-American-Monsoon	13.79°S	60.56°W
14	SWS	S.W.South-America	30.03°S	71.06°W
15	SES	S.E.South-America	28.72°S	58.04°W
16	SSA	S.South-America	48.13°S	69.50°W
17	NEU	N.Europe	61.63°N	17.59°E
18	WCE	West&Central-Europe	51.37N	22.60°E
19	EEU	E.Europe	55.00°N	50.00°E
20	MED	Mediterranean	37.96°N	14.53°E
21	SAH	Sahara	21.67°N	10.52°E
22	WAF	Western-Africa	9.49°N	0.85°W
23	CAF	Central-Africa	1.67°N	18.46°E
24	NEAF	N.Eastern-Africa	7.99°N	37.96°E
25	SEAF	S.Eastern-Africa	3.70°S	33.74°E
26	WSAF	W.Southern-Africa	21.25°S	18.69°E
27	ESAF	E.Southern-Africa	19.85°S	30.89°E
28	MDG	Madagascar	19.67°S	46.56°E
29	RAR	Russian-Arctic	70.41°N	108.00°E
30	WSB	W.Siberia	56.00°N	75.00°E
31	ESB	E.Siberia	56.00°N	110.00°E
32	RFE	Russian-Far-East	58.88°N	148.96°E
33	WCA	W.C.Asia	37.23°N	57.17°E
34	ECA	E.C.Asia	42.13°N	93.56°E
35	TIB	Tibetan-Plateau	32.97°N	87.00°E
36	EAS	E.Asia	33.93°N	117.83°E
37	ARP	Arabian-Peninsula	22.35°N	46.92°E

38	SAS	S.Asia	22.70°N	79.91°E
39	SEA	S.E.Asia	3.01°N	116.49°E
40	NAU	N.Australia	16.20°S	134.82°E
41	CAU	C.Australia	25.17°S	129.93°E
42	EAU	E.Australia	27.72°S	149.64°E
43	SAU	S.Australia	34.33°S	134.71°E
44	NZ	New-Zealand	42.08°S	171.92°E